

Quantum entanglement recognition

Jun Yong Khoo¹ and Markus Heyl¹

¹*Max-Planck Institute for the Physics of Complex Systems, D-01187 Dresden, Germany*

(Dated: July 30, 2020)

Entanglement constitutes a key characteristic feature of quantum matter. Its detection, however, still faces major challenges. In this letter, we formulate a framework for probing entanglement based on machine learning techniques. The central element is a protocol for the generation of statistical images from quantum many-body states, with which we perform image classification by means of convolutional neural networks. We show that the resulting quantum entanglement recognition task is accurate and can be assigned a well-controlled error across a wide range of quantum states. We discuss the potential use of our scheme to quantify quantum entanglement in experiments. Our developed scheme provides a generally applicable strategy for quantum entanglement recognition in both equilibrium and nonequilibrium quantum matter.

I. INTRODUCTION

Entanglement has turned into a central concept across various branches in physics ranging from quantum technological applications [1] to the characterization of quantum matter [2, 3]. It has remained, however, a key challenge to quantify the entanglement content of a given quantum state especially under realistic experimental conditions beyond the ground and pure state paradigm. This challenge is rooted in the fundamental property that entanglement measures are nonlinear functions of the density matrix, but quantum measurements only yield direct information linear in it according to the axiomatic foundations of quantum mechanics. For quantum systems involving a limited number of degrees of freedom, entanglement can still be quantified also experimentally upon reconstructing the full density matrix via tomography [4–8], by means of measurements on identical copies of quantum states [9–13], or through the statistics of randomized measurements [14–16].

By applying machine learning techniques we show in this work that entanglement measures can be accurately extracted merely from limited information linear in the system's density matrix, thereby reducing significantly the necessary measurement resources. The key element of the proposed scheme is a protocol to generate a two-dimensional statistical image from a given quantum many-body state. Utilizing conventional image recognition based on convolutional neural networks we then perform a quantitative classification of the entanglement entropy and logarithmic negativity, ranging over a broad class of quantum many-body wave functions from ground and excited states to quantum nonequilibrium evolution for pure and mixed states. We apply these techniques to various one-dimensional quantum spin-1/2 chains and find that this classification is remarkably accurate and can be assigned a well-defined error. Importantly, we find that the artificial neural networks (ANNs) for quantum entanglement recognition can generalize, which we study quantitatively across different kinds of spin chains. In particular, the obtained ANNs can, at a controlled error, even predict nonequilibrium dynamics, generated

e.g. by a Lindblad-master equation, despite not having seen such an evolution before. We further discuss how this quantum entanglement recognition might be utilized experimentally as an entanglement estimator upon training with simulated data.

II. IMAGE GENERATION FROM QUANTUM STATES

The key element of our quantum entanglement recognition scheme is the statistical image generating protocol, which we now introduce. Let ρ_0 denote the density matrix of a quantum (many-body) system. In the following, we study models of L spin-1/2 degrees of freedom for simplicity, although the protocol can be extended straightforwardly to any lattice model with finite local Hilbert spaces. We perform measurements on the quantum state with the string $O = \sigma_1^z \otimes \dots \otimes \sigma_L^z$ of Pauli matrices σ_l^z yielding as outcomes spin configurations $\mathbf{s} = (s_1, \dots, s_L)$ with $s_l = \pm 1$. Such measurements can be performed in quantum computing platforms such as trapped ions [17] and superconducting qubits [18–20] or ultra-cold atomic systems via quantum gas microscopes [21]. In general, a single measurement basis is not sufficient for entanglement detection. We therefore generate a more detailed picture of ρ_0 by applying a set of \mathcal{W} fixed but random local unitary transformations $U_i = u_{i,1} \otimes \dots \otimes u_{i,L}$ with $i = 1, \dots, \mathcal{W}$, where each local unitary $u_{i,l}$ on site l is drawn independently from the circular unitary ensemble (CUE) [22]. Measuring the rotated $\rho \mapsto \rho^i = U_i \rho_0 U_i^\dagger$ as before we obtain the probabilities

$$p_{ij} = \langle j | \rho^i | j \rangle = \text{Tr} \left[U_i \rho_0 U_i^\dagger |j\rangle \langle j| \right], \quad (1)$$

with $j = 1, \dots, \mathcal{D}$ labeling the $\mathcal{D} = 2^L$ spin configurations. In this way we obtain a two-dimensional representation of ρ_0 in terms of the probabilities p_{ij} , shown for three exemplary states of different entanglement classes in Fig. 1(a).

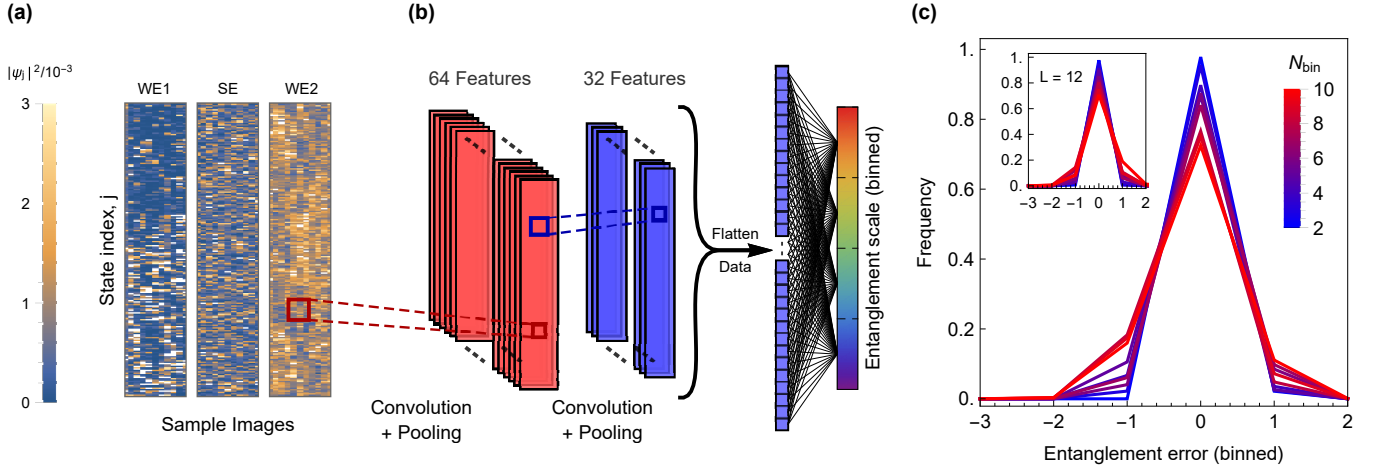


FIG. 1. Schematic illustration of the quantum entanglement recognition scheme. (a) Representative statistical images of weakly entangled pure states (WE1), strongly entangled pure states (SE) and weakly entangled mixed states (WE2) of the transverse-field ferromagnetic Ising model. (b) Adapting an image recognition neural network for entanglement quantification. The network reads statistical images such as those in (a). After processing the image information the network classifies the entanglement by assigning the images to different labels corresponding to binned intervals of the considered entanglement measure. In the shown case this is for the case of a total number $N_{\text{bin}} = 4$ of bins. (c) Distribution of the error in entanglement quantification for ground states of the ferromagnetic transverse-field Ising model (WE1) over a range of $2 \leq N_{\text{bin}} \leq 10$. Error distances δ are measured in units of bins.

III. SUPERVISED LEARNING OF ENTANGLEMENT

In the following we now outline how the introduced statistical image generation can be used to perform a quantitative entanglement classification task by means of a supervised learning procedure. For pure states a natural entanglement measure is the half-chain entanglement entropy

$$S(\rho) = -\text{Tr}_< [\rho_< \ln \rho_<], \quad (2)$$

with $\rho_< = \text{Tr}_> \rho$ the reduced density for the first half of the chain, obtained by tracing out the degrees of freedom of the remainder $>$ from the full density matrix ρ . For mixed states we use instead the logarithmic negativity [23],

$$E_{\mathcal{N}}(\rho) = \log_2 \|\rho^{T<}\|, \quad (3)$$

where $\|\rho^{T<}\|$ denotes the trace norm of $\rho^{T<}$ and $\rho^{T<}$ is the partial transpose of ρ on the degrees of freedom of the first half of the chain.

For the desired quantification task we bin the range of values for the respective entanglement measure into N_{bin} equally-spaced intervals. We fix an interval $I_S = [0, S_{\text{max}}]$ for the entanglement entropy S , say, with a suitably chosen S_{max} and decompose $I_S = \bigcup_{n=1}^{N_{\text{bin}}} I_{S_n}$ into $I_{S_n} = [(n-1)\Delta S, n\Delta S)$ with $n = 1, \dots, N_{\text{bin}} = S_{\text{max}}/\Delta S$. Each of these bins, labeled by n , corresponds to the category to which we aim to associate the images. With this we can now perform an entanglement classification problem as in conventional image recognition. We adapt a convolutional neural network to process the

two-dimensional image of the quantum state as shown in Fig. 1(b), for details see Appendix A. We quantify the classification accuracy on test images by the signed binning error distance $\delta = n - n_{\text{ANN}}$ measuring the difference between the bin label n from the exact entanglement content and n_{ANN} predicted by the ANN. A typical distribution of δ for various $2 \leq N_{\text{bin}} \leq 10$ is shown in Fig. 1(c) for a specific benchmark problem. Importantly, the entanglement classification exhibits a well-defined error, whose distribution is sharply peaked around $\delta = 0$, implying no error, with some further appreciable weight only for $\delta = \pm 1$.

IV. RESULTS

It is the key goal of the following analysis to explore the performance of the quantum entanglement recognition scheme for a large variety of quantum states.

A. Models

As benchmark systems we choose a set of paradigmatic one-dimensional quantum many-body models. This includes the transverse-field Ising chain with either ferromagnetic (TFI+) or antiferromagnetic (TFI-) couplings

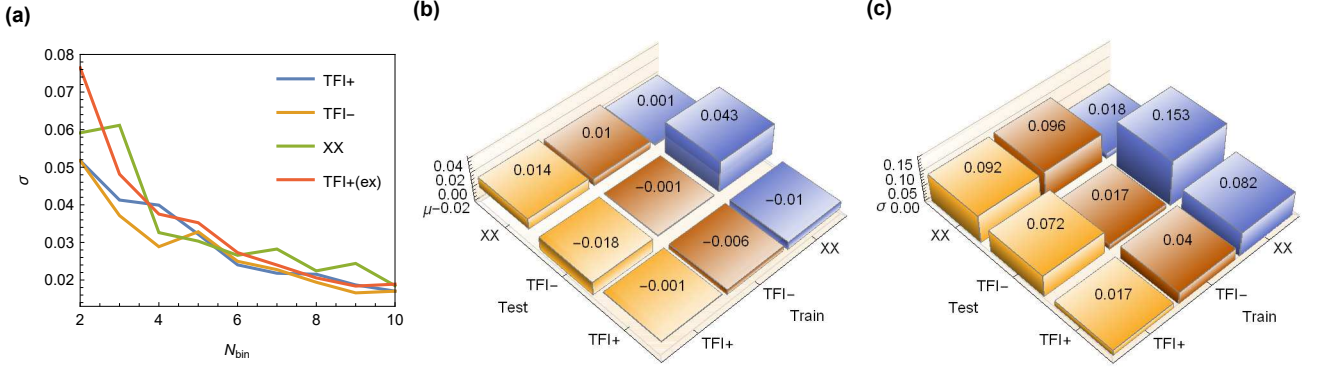


FIG. 2. Characterization of network performance on weakly entangled states. (a) The rescaled standard deviation σ of the binning error made by the trained network decreases as the total number of bins N_{bin} used for the training increases. The binning error is rescaled by N_{bin} to reflect the reduction in the maximum entanglement entropy error as N_{bin} increases. The plots are shown for the case when the network is tested on the same class of entangled states it was trained on. The three classes of weakly-entangled ground states considered are those from the transverse field ferromagnetic (TFI+) and antiferromagnetic (TFI-) Ising models as well as the XX model. Shown also is the corresponding plot for the full spectrum of TFI+ excited states (red), indicating the network’s ability to generalize and quantify beyond area-law type entanglement. (b) The rescaled mean μ and (c) the rescaled standard deviation σ of the binning error of the network for all possible training/test combinations from these three classes. The results shown are for the case of $N_{\text{bin}} = 10$.

as well as the XX model:

$$H_{\text{TFI}\pm} = \mp \sum_{\langle i,j \rangle} \sigma_i^x \sigma_j^x - h \sum_{i=1}^L \sigma_i^z, \quad (4)$$

$$H_{\text{XX}} = - \sum_{\langle i,j \rangle} (\sigma_i^x \sigma_j^x + \sigma_i^y \sigma_j^y) - h \sum_{i=1}^L (-1)^i \sigma_i^z. \quad (5)$$

Here, $\sigma_i^{x,y,z}$ denote the Pauli matrices at site $i = 1, \dots, L$ and h a magnetic field strength. While throughout this work we show numerical data for $L = 10$, we emphasize that the entanglement recognition does not depend significantly on L , as exemplified in Fig. 1(c) where we also include data for $L = 12$. Although we focus on a particular set of models, we find that our results do not depend crucially on the model details as discussed below, suggesting that our observations are generic and therefore applicable in broad context.

B. Ground and excited states

We start by studying weakly entangled ground states of the considered spin chains. First, we explore the performance by testing on the same class of states, e.g., with ground states of TFI+ after training the ANN with ground states of the same model (see Appendix B for details). The network performs remarkably well in this case, as can be seen in Fig. 1(c) showing a typical distribution of the binning error δ . Almost independent of N_{bin} , one can recognize a strongly peaked distribution with an appreciable weight beyond $\delta = 0$ only at $\delta = \pm 1$. As the mean error is practically vanishing, the performance is effectively captured by the standard deviation, which can therefore be used as a well-defined error

quantifier. The fact, that the network typically fails at most by assigning a state to the nearest-neighboring bin, suggests that the dominant error originates from those instances where the actual entanglement entropy resides close to the border between two bins. A particularly important consequence of Fig. 1(c) is that the performance of the network improves upon enlarging N_{bin} . This can be quantified by $\delta S = S_n - S_n^{\text{ANN}} = \delta \times \Delta S$, where S_n denotes the binned value of the computed entanglement entropy and S_n^{ANN} the one predicted by the ANN. The result for the corresponding standard deviation σ of $\delta S/S_{\text{max}}$ is shown in Fig. 2(a) for all the different models considered, showing a clear improvement in network prediction accuracy for larger N_{bin} .

As a next step we aim to explore the capabilities of the ANN to generalize to unfamiliar data by testing the network with states from model classes different to those it was trained on. Remarkably, the distributions for δ exhibit the same structure as in Fig. 1(c). The respective summary on all training/test combinations is shown in Fig. 2(b,c) for $N_{\text{bin}} = 10$ containing both the mean μ and the standard deviation σ of $\delta S/S_{\text{max}}$. As expected, the network performs best when tested on the same class of states it was trained on. However, it can also generalize to different states, albeit with a slightly poorer performance, suggesting that the ANN indeed learns about some universal features of quantum entanglement. We further point out that our scheme also applies to excited states with volume-law entanglement, where we again find a strongly peaked distributions for δ . We have included for one representative case, $H_{\text{TFI+}}$, the corresponding σ in Fig. 2(a). We have also checked that the network performs equally well when making the Ising chain nonintegrable and across different entanglement measures (see Appendix D for details).

C. Generalizing to unitary time evolution

As a next step we aim to explore quantum entanglement recognition in nonequilibrium dynamics. This is of particular importance for many quantum simulator platforms, where it is much more natural to realize time evolution than for instance ground state preparation. Here, we will be exclusively interested in whether the ANN trained on an image library composed out of $H_{\text{TFI}+}$ eigenstates and random product states is capable of generalizing to dynamics. For details see Appendix B and C. As a benchmark, we consider the evolution of randomly polarized states under $H_{\text{TFI}+}$. The resulting prediction for the entanglement entropy $S_n^{\text{ANN}}(t)$ (green curve), based on its statistical image time series, in comparison to the exact real-time evolution $S(t)$ (black curve) is shown in Fig. 3(a) for a specific instance (dashed lines) and averaged over 100 different initial randomly polarized states (solid lines) with a shaded region indicating the associated standard deviation. As one can see, the network recognizes the essential features of the dynamics such as the fast initial growth or even the temporal fluctuations in the long-time dynamics.

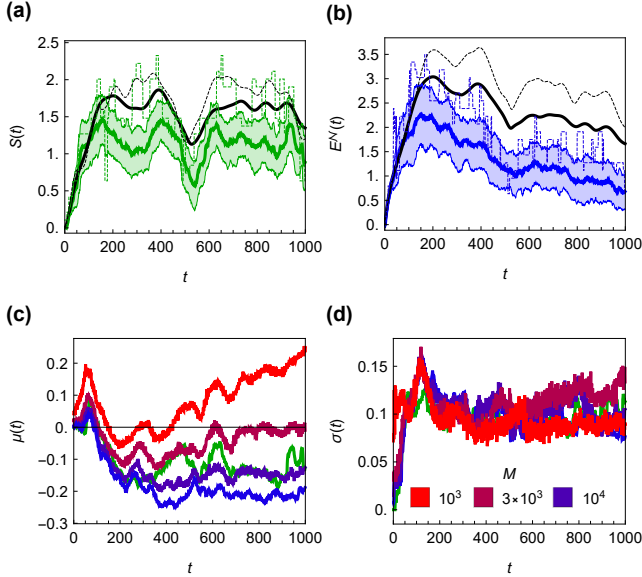


FIG. 3. Quantifying dynamics of entanglement. (a) Unitary dynamics of the entanglement entropy $S(t)$ and (b) dissipative dynamics of the logarithmic negativity $E_N(t)$, for a representative initial random polarized state (thin dashed lines) and averaged over 100 different initial randomly polarized states (solid lines). Network prediction is given in green and blue respectively, with a shaded region indicating the associated standard deviation over the initial random states. (c) The mean $\mu(t)$ and (d) standard deviation $\sigma(t)$ of the respective rescaled entanglement errors taken over the 100 initial states used to produce the plots in (a) and (b). Color variation from blue (noiseless) to red indicates the level of noise introduced to the statistical image time series via finite M sampling – $M = 10^4$ (purple), $M = 3000$ (magenta), $M = 1000$ (red).

D. Generalizing to dissipative dynamics

In an experimentally realistic context the major challenge is to quantify entanglement for mixed states. For this purpose we study exemplarily the logarithmic negativity E_N for non-unitary time evolution as described by a Lindblad master equation of the form $\partial_t \rho = -i[H_{\text{TFI}+}, \rho] + \gamma \sum_{i=1}^L (\sigma_i^x \rho \sigma_i^x - \rho)$ with γ characterizing the dissipation strength. For the training library, in addition to the eigenstates of $H_{\text{TFI}+}$, it turns out to be important to also include images for two new classes – separable mixed states, and states generated by evolving eigenstates of $H_{\text{TFI}+}$ only with the dissipative part of the master equation (see Appendix B for details). The performance of the network trained with all three classes of images is shown in Fig. 3(c,d). We find that the ANN is capable of accurately tracking the evolution of E_N for the studied dissipative dynamics. Analogous to the purely unitary case, we compare in Fig. 3(b) the network-predicted $E_{N,n}^{\text{ANN}}(t)$ (blue curves) to the exact result $E_N(t)$ (black curves) for the case of weak dissipative dynamics with $\gamma = 0.01$. For early times $t < 100 \sim \gamma^{-1}$, the evolution is approximately unitary and $E_N(t)$ increases linearly with time. At later times $t > 100$ however, $E_N(t)$ gradually decays as dissipation kicks in leading to a reduction of entanglement. The network performs comparably well to the unitary case, where in both cases it begins to underpredict the entanglement present at $t > 100$. We characterize the average performance of the network by the time-dependent mean $\mu(t)$ [Fig. 3(c)] and standard deviation $\sigma(t)$ [Fig. 3(d)] of the rescaled entanglement errors $\delta S_n^{\text{ANN}}(t)/S_{\text{max}}$ for the unitary case and $\delta E_{N,n}^{\text{ANN}}(t)/E_{N,\text{max}}$ for the non-unitary case, taken over 100 different initial randomly polarized states.

V. SUMMARY AND DISCUSSION

In this work we have introduced quantum entanglement recognition based on machine learning techniques. Our protocol provides a controlled and unbiased way to extract quantum state information by essentially applying projective measurements in \mathcal{W} predetermined but randomly selected bases. By organizing these information into a statistical image, the entanglement quantification task is mapped into the conventional image recognition task, for which convolutional neural networks have been optimized to achieve excellent performance. In the large $\mathcal{W} \sim 2^L$ limit, these statistical images essentially capture all the information present in the density matrix, such that it would not be surprising if a trained convolutional neural network is able to successfully reconstruct the entanglement associated to a statistical image.

The central result of this work is to show that indeed the above expectation is correct, and more remarkably, only a small set of measurement bases $\mathcal{W} \ll 2^L$ is required. This is the key feature going beyond previous works on applying machine learning techniques to char-

acterize quantum matter [24–28], which operate either in a single measurement basis [24, 25, 27, 28] or by considering low-order correlation functions [26]. By applying to various different classes of quantum many-body states we show that the resulting quantum entanglement recognition can be assigned a well-defined error making the scheme accurate and reliable. We further show that the networks in our scheme are capable of generalizing to, e.g., nonequilibrium dynamics, implying that the networks can learn universal features of quantum entanglement, and from a theoretical standpoint, that such features are already well-encoded within the state information obtained from $\mathcal{W} \ll 2^L$ measurement bases. A generalizable network is particularly important for its potential use in experiments, where the microscopic details of the dynamics might not be known in full detail.

In the experimental context, the probabilities p_{ij} from Eq. (1) can only be estimated from a finite number of measurements M onto spin configurations, introducing noise onto the statistical images. In Fig. 3(c,d), we have included results for such noisy images where one can see that even with $M = 3000$ per rotation the dynamics can be reproduced well. For the considered $\mathcal{W} = 5$ rotations this implies a total number of 15000 measurements, which is much less compared to a recent experiment on probing Renyi entropies [16]. Let us emphasize, however, that we have not attempted to optimize the ANN for the entanglement recognition task at finite M , so that further improvements at this front will likely appear in the future. This opens the door to the development of machine learning tools that directly enable experimental studies on quantum entanglement in systems beyond the few body context. This is all the more important as many phases of strongly correlated quantum matter are characterized by their entanglement content such as in, e.g., quantum spin liquids.

VI. ACKNOWLEDGEMENTS

This project has received funding from the European Research Council (ERC) under the European Unions Horizon 2020 research and innovation programme (grant agreement No. 853443), and M. H. further acknowledges support by the Deutsche Forschungsgemeinschaft via the Gottfried Wilhelm Leibniz Prize program.

Appendix A: Convolutional neural networks for entanglement recognition

Based on the statistical images generated out of quantum many-body states, we perform a conventional image recognition task using a convolutional neural network. For all the shown data the network consists of two convolution layers and a hidden dense layer fully connected to the different output categories established by the different image labels. The first convolution layer scans a sta-

tistical image and constructs 64 different feature maps, which are in turn scanned by the second layer to construct 32 new feature maps. This feature information is then flattened to form the dense layer, which is in turn fitted across the images from the training library to their respective N_{bin} labels.

Appendix B: Training libraries

For unbiased training of the ANN, the training library is constructed by generating an approximately equal number of widely varied reference images in each of the N_{bin} categories, i.e. images from states with entanglement spread across I_{S_n} for each bin n .

1. Ground states:

We solve for the ground states for different magnetic field strengths $h > 1$ for each of the model classes to obtain the corresponding libraries of labeled images with a uniformly distributed entanglement entropy $S \in I_S = [0, \ln 2]$. To ensure that there are no directional biases in the images concerning a specific orientation on the Bloch sphere, a uniform random rotation $U = \otimes_{i=1}^L u_i$ is applied to each state before generating its corresponding statistical image. We separately train the ANN with the library of a particular model class and then test the entanglement classification with new states it has not seen before either from the same or a different model class. Each training library contains 50000 images, while an additional 10000 images are generated for each test library.

2. Excited states:

We focus on the TFI+ model (as well as a non-integrable modification) for the study of excited states. We solve for the eigenstates and their corresponding entanglement entropies (also logarithmic negativities) for a range of near critical field strengths $h \in (1, 1.07)$. For each h -value, the eigenstates are grouped into N_{bin} bins ranging between their maximum and minimum entanglement entropies. One state is randomly selected from each bin for image generation, while the rest of the eigenstates are discarded.

3. Unitary dynamics:

In addition to the TFI+ ground and excited state images, it is important to also include random product states, defined as $|RP\rangle = |\hat{n}_1\rangle \otimes \dots \otimes |\hat{n}_L\rangle$ where $|\hat{n}_i\rangle$ denotes a spin-1/2 state at site i pointing along a random unit vector \hat{n}_i on the Bloch sphere. Once again we generate 50000 $|RP\rangle$ images, for a total of 150000 images on which we train the ANN.

4. Dissipative dynamics:

Two new classes of images are required for this task in addition to the TFI+ ground and excited state images. The first class is random separable mixed states defined as $\rho^{SP} = \sum_{\alpha} p_{\alpha} |RP\rangle_{\alpha} \langle RP|_{\alpha}$ where $\{|RP\rangle_{\alpha=1, \dots, \alpha_{\max}}\}$ are α_{\max} instances of random product states and $\sum_{\alpha} p_{\alpha} = 1$. We considered uniformly distributed values of $2 \leq \alpha_{\max} \leq 20$. This class generalizes the $|RP\rangle$ used for the unitary case. The second class of states are ‘dissipated TFI+’ states ρ^{DTFI+} . These states are generated by evolving eigenstates of H_{TFI+} only with the dissipative part of the master equation $\partial_t \rho = \gamma \sum_{i=1}^L (\sigma_i^x \rho \sigma_i^x - \rho)$ with $\gamma = 0.1$, from short to long times relative to the decay of their initial E_N values. The procedure starts off as per the TFI+ excited state images. For each of the N_{bin} selected excited states, the state and E_N decay is tracked throughout the dissipation. These dissipated states are grouped into N_{bin} bins ranging between the maximum and minimum E_N during the dissipation. One state is randomly selected from each bin for image generation, while the rest are discarded. For each h value, a total of N_{bin}^2 states are selected for image generation. While artificially constructed, statistical images of these states contain the crucial features that allow the trained network to distinguish between superpositions of highly entangled states, obtained for instance from late times of unitary time evolution, and highly mixed states with low entanglement. 50000 ρ^{SP} and 100000 ρ^{DTFI+} images are generated, for a total of 250000 images on which we train the ANN.

Appendix C: Solving the unitary and dissipative dynamics

The time evolution of a given initial state is numerically solved by employing the `mesolve` function of QuTiP (Quantum Toolbox in Python) [29, 30].

Appendix D: Network Performance on excited states of Non-Integrable Ising Model based on different entanglement measures

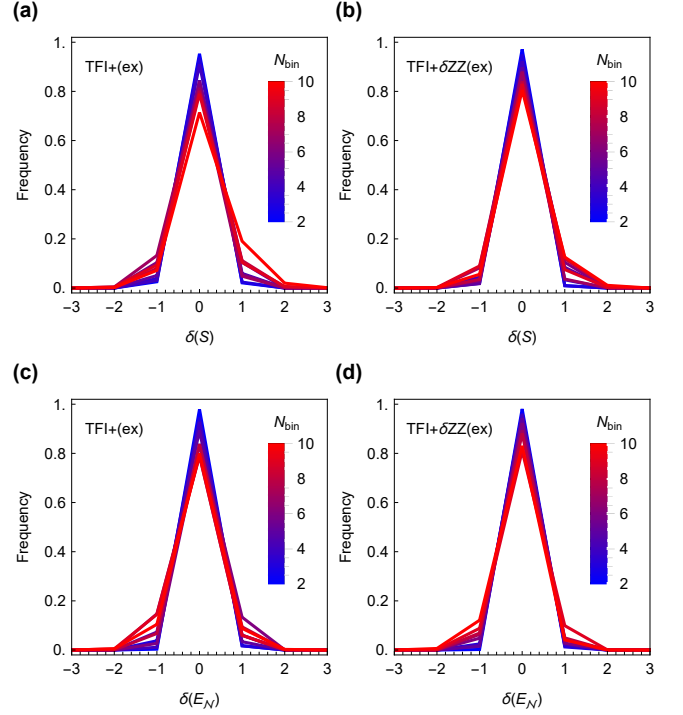


FIG. 4. Distribution of the error in entanglement quantification for excited states of the (a, c) ferromagnetic transverse-field Ising model H_{TFI+} , and (b, d) a non-integrable version of it, $\tilde{H}_{TFI+} = H_{TFI+} + 0.2 \sum_{\langle i,j \rangle} \sigma_i^z \sigma_j^z$, over a range of $2 \leq N_{\text{bin}} \leq 10$. The network accurately quantifies entanglement independent on the entanglement measure, where in (a, b) the network was trained on images labeled by their half-chain entanglement entropy S (binned), while in (c, d) by their half-chain logarithmic negativity E_N (binned). The respective error distances δ are measured in units of bins.

-
- [1] Jonathan P. Dowling and Gerard J. Milburn, “Quantum technology: the second quantum revolution,” *Philosophical Transactions of the Royal Society of London Series B* **364**, 1674–1679 (2009).
- [2] Luigi Amico, Rosario Fazio, Andreas Osterloh, and Vlatko Vedral, “Entanglement in many-body systems,” *Rev. Mod. Phys.* **80**, 517–576 (2008).
- [3] Nicolas Laflorencie, “Quantum entanglement in condensed matter systems,” *Physics Reports* **646**, 1 – 59 (2016).
- [4] K. Kim, M.-S. Chang, S. Korenblit, R. Islam, E. E. Edwards, J. K. Freericks, G.-D. Lin, L.-M. Duan, and C. Monroe, “Quantum simulation of frustrated ising spins with trapped ions,” *Nature* **465**, 590–593 (2010).
- [5] P. Jurcevic, B. P. Lanyon, P. Hauke, C. Hempel, P. Zoller, R. Blatt, and C. F. Roos, “Quasiparticle engineering and entanglement propagation in a quantum many-body system,” *Nature* **511**, 202–205 (2014).
- [6] T. Lanting, A. J. Przybysz, A. Yu. Smirnov, F. M. Spedalieri, M. H. Amin, A. J. Berkley, R. Harris, F. Altomare, S. Boixo, P. Bunyk, N. Dickson, C. Enderud, J. P. Hilton, E. Hoskinson, M. W. Johnson, E. Ladizinsky, N. Ladizinsky, R. Neufeld, T. Oh, I. Perminov, C. Rich, M. C. Thom, E. Tolkacheva, S. Uchaikin, A. B. Wilson, and G. Rose, “Entanglement in a quantum annealing processor,” *Phys. Rev. X* **4**, 021041 (2014).
- [7] Takeshi Fukuhara, Sebastian Hild, Johannes Zeiher, Peter Schauß, Immanuel Bloch, Manuel Endres, and Christian Gross, “Spatially resolved detection of a spin-entanglement wave in a bose-hubbard chain,” *Phys. Rev. Lett.* **115**, 035302 (2015).
- [8] B. P. Lanyon, C. Maier, M. Holzäpfel, T. Baumgratz, C. Hempel, P. Jurcevic, I. Dhand, A. S. Buyskikh, A. J. Daley, M. Cramer, M. B. Plenio, R. Blatt, and C. F. Roos, “Efficient tomography of a quantum many-body system,” *Nature Physics* **13**, 1158–1162 (2017).
- [9] A. J. Daley, H. Pichler, J. Schachenmayer, and P. Zoller, “Measuring entanglement growth in quench dynamics of bosons in an optical lattice,” *Phys. Rev. Lett.* **109**, 020505 (2012).
- [10] Dmitry A. Abanin and Eugene Demler, “Measuring entanglement entropy of a generic many-body system with a quantum switch,” *Phys. Rev. Lett.* **109**, 020504 (2012).
- [11] Rajibul Islam, Ruichao Ma, Philipp M. Preiss, M. Eric Tai, Alexander Lukin, Matthew Rispoli, and Markus Greiner, “Measuring entanglement entropy in a quantum many-body system,” *Nature* **528**, 77–83 (2015).
- [12] Adam M. Kaufman, M. Eric Tai, Alexander Lukin, Matthew Rispoli, Robert Schittko, Philipp M. Preiss, and Markus Greiner, “Quantum thermalization through entanglement in an isolated many-body system,” *Science* **353**, 794–800 (2016).
- [13] Alexander Lukin, Matthew Rispoli, Robert Schittko, M. Eric Tai, Adam M. Kaufman, Soonwon Choi, Vedika Khemani, Julian Léonard, and Markus Greiner, “Probing entanglement in a many-body-localized system,” *Science* **364**, 256–260 (2019).
- [14] S. J. van Enk and C. W. J. Beenakker, “Measuring $\text{Tr}\rho$ on single copies of ρ using random measurements,” *Phys. Rev. Lett.* **108**, 110503 (2012).
- [15] A. Elben, B. Vermersch, M. Dalmonte, J. I. Cirac, and P. Zoller, “Rényi entropies from randomized quenches in the hubbard and spin models,” *Phys. Rev. Lett.* **120**, 050406 (2018).
- [16] Tiff Brydges, Andreas Elben, Petar Jurcevic, Benoît Vermersch, Christine Maier, Ben P. Lanyon, Peter Zoller, Rainer Blatt, and Christian F. Roos, “Probing rényi entanglement entropy via randomized measurements,” *Science* **364**, 260–263 (2019).
- [17] R. Blatt and C. F. Roos, “Quantum simulations with trapped ions,” *Nature Physics* **8**, 277–284 (2012).
- [18] T. Walter, P. Kurpiers, S. Gasparinetti, P. Magnard, A. Potočnik, Y. Salathé, M. Pechal, M. Mondal, M. Oppliger, C. Eichler, and A. Wallraff, “Rapid high-fidelity single-shot dispersive readout of superconducting qubits,” *Phys. Rev. Applied* **7**, 054020 (2017).
- [19] Johannes Heinsoo, Christian Kraglund Andersen, Ants Remm, Sebastian Krinner, Theodore Walter, Yves Salathé, Simone Gasparinetti, Jean-Claude Besse, Anton Potočnik, Andreas Wallraff, and Christopher Eichler, “Rapid high-fidelity multiplexed readout of superconducting qubits,” *Phys. Rev. Applied* **10**, 034040 (2018).
- [20] S. Touzard, A. Kou, N. E. Frattini, V. V. Sivak, S. Puri, A. Grimm, L. Frunzio, S. Shankar, and M. H. Devoret, “Gated conditional displacement readout of superconducting qubits,” *Phys. Rev. Lett.* **122**, 080502 (2019).
- [21] Stefan Kuhr, “Quantum-gas microscopes: a new tool for cold-atom quantum simulators,” *National Science Review* **3**, 170–172 (2016).
- [22] Francesco Mezzadri, “How to generate random matrices from the classical compact groups,” *Notices of the American Mathematical Society* **54** (2006).
- [23] G. Vidal and R. F. Werner, “Computable measure of entanglement,” *Phys. Rev. A* **65**, 032314 (2002).
- [24] Juan Carrasquilla and Roger G. Melko, “Machine learning phases of matter,” *Nature Physics* **13**, 431–434 (2017).
- [25] Kelvin Ch’ng, Juan Carrasquilla, Roger G. Melko, and Ehsan Khatami, “Machine learning phases of strongly correlated fermions,” *Physical Review X* **7**, 031038 (2017).
- [26] Peter Broecker, Juan Carrasquilla, Roger G. Melko, and Simon Trebst, “Machine learning quantum phases of matter beyond the fermion sign problem,” *Scientific Reports* **7**, 8823 (2017).
- [27] Iris Cong, Soonwon Choi, and Mikhail D. Lukin, “Quantum convolutional neural networks,” *Nature Physics* **15**, 1273–1278 (2019).
- [28] Annabelle Bohrdt, Christie S. Chiu, Geoffrey Ji, Muqing Xu, Daniel Greif, Markus Greiner, Eugene Demler, Fabian Grusdt, and Michael Knap, “Classifying snapshots of the doped hubbard model with machine learning,” *Nature Physics* **15**, 921–924 (2019).
- [29] J.R. Johansson, P.D. Nation, and Franco Nori, “Qutip: An open-source python framework for the dynamics of open quantum systems,” *Computer Physics Communications* **183**, 1760 – 1772 (2012).
- [30] J.R. Johansson, P.D. Nation, and Franco Nori, “Qutip 2: A python framework for the dynamics of open quantum systems,” *Computer Physics Communications* **184**, 1234 – 1240 (2013).